

---

# Reusable Slotwise Mechanisms

---

Trang Nguyen<sup>1,2</sup> Amin Mansouri<sup>1</sup> Kanika Madan<sup>1</sup> Khuong Nguyen<sup>2</sup> Kartik Ahuja<sup>1</sup> Dianbo Liu<sup>1</sup>  
Yoshua Bengio<sup>1,3,4</sup>

## Abstract

Agents that can understand and reason over the dynamics of objects can have a better capability to act robustly and generalize to novel scenarios. Such an ability, however, requires a suitable representation of the scene as well as an understanding of the mechanisms that govern the interactions of different subsets of objects. To address this problem, we propose Reusable Slotwise Mechanisms, or RSM, that jointly learns a slotwise representation of the scene and a modular architecture that dynamically chooses one mechanism among a set of reusable mechanisms to predict the next state of each slot. RSM crucially takes advantage of a *Central Contextual Information (CCI)*, which lets each selected reusable mechanism access the rest of the slots through a bottleneck, effectively allowing for modeling higher order and complex interactions that might require a sparse subset of objects. We show how this model outperforms state-of-the-art methods in a variety of next-step prediction tasks ranging from grid-world environments to Atari 2600 games. Particularly, we challenge methods that model the dynamics with Graph Neural Networks (GNNs) on top of slotwise representations, and modular architectures that restrict the interactions to be only pairwise. Finally, we show that RSM is able to generalize to scenes with objects varying in number and shape, highlighting its out-of-distribution generalization capabilities. Our implementation is available online<sup>1</sup>.

## 1. Introduction

Reasoning over the objects, such as in a video, and predicting the future frames are essential for many computer vision tasks. Such capabilities can be the foundation for the construction of rich world models in applications such as

<sup>1</sup>Mila, Quebec AI Institute, Canada <sup>2</sup>FPT Software AI Center, Vietnam <sup>3</sup>CIFAR AI Chair <sup>4</sup>University of Montreal, Quebec, Canada. Correspondence to: Trang Nguyen <trangphuongnguyen@gmail.com>.

autonomous driving and reinforcement learning for robots. These tasks require an agent to acquire a good representation of the scene that can then be used to analyze how different parts relate to each other. Traditionally, a large number of deep learning-based representation learning methods compress the whole scene into a monolithic representation, i.e., a single feature vector. Despite their success in some tasks, lack of compositionality and ignoring the object-centric aspect of natural scenes make it difficult for these monolithic representations to attain systematic generalization and interpretability. Moreover, such representations entangle causal variables in non-trivial ways, making it complicated to understand interactions between different objects and can lead to poor generalization. Recently, methods based on slot-based and modular representations that decompose the scene into entities have seen a surge in interest, while departing from fixed-size monolithic feature vector representations (Graves et al., 2014; Santoro et al., 2018; Goyal et al., 2020; 2021a; Goyal & Bengio, 2020; Goyal et al., 2021b; Madan et al., 2021; Henaff et al., 2017; Li et al., 2018; Rosenbaum et al., 2019; Shazeer et al., 2017; Fernando et al., 2017; Liu et al., 2022). These slot-based representations that decompose the input form the basis for this work. An encoder that segments a scene into its independent constituent entities instead of compressing the abundance of information into a fixed-size representation provides much more flexibility when dealing with a varying number of objects. At the same time, parameter sharing, when learning object-centric representations, would help reuse persistent patterns across object properties, making such representations suitable for generalization. Such compositional and object-centric representations can then be used with complex world models that capture the interactions and evolution of different entities.

These world models, when presented with proper representations, in principle, can model the transition functions that relate latent causal factors across consecutive time steps of a rollout. Although monolithic blocks are still occasionally used with object-centric methods (Wu et al., 2022), there have been a number of attempts to incorporate similar inductive biases (related to the object-centricity of the images) in modeling the interactions. The importance of such *structured* world models and representations is due to the potential they provide for systematic generalization to novel scenes. Similar to a structured representation, a structured world model that decomposes the description of the evolution of a scene into causal and independent sub-modules

<sup>1</sup>[github.com/trangnnp/RSM](https://github.com/trangnnp/RSM)

can easily recombine and re-purpose those mechanisms in novel ways to solve the challenges in an unseen scenario. Furthermore, such world models can be adapted for sample efficiently; for example, if the parameters of one mechanism change in a new environment, unlike a monolithic architecture, we do not need to re-train the whole model from scratch; rather, smaller updates to only the changed components should be sufficient to achieve good performance in the new setting.

Among attempts at augmenting world models with such priors, most notably, a class of algorithms bakes in the assumption that the transition functions transforming a latent representation to the next step can be modeled through only pairwise interactions. A subclass of this group leverages GNNs to learn such dependencies, which predispose connections among objects to be dense. Additionally, a GNN brings along another restriction, where the interactions can only be modeled through node and edge update functions, whereas physical laws giving rise to a dynamic scene usually comprise a few rules (not just two), which ideally, an agent should learn to choose from and reuse depending on the context and each object. Thus, a modular architecture design for modeling transitions seems essential.

In this work, we argue why assumptions made in previous attempts at learning the dynamics among slots can be insufficient in more realistic domains, and to address them, we introduce Reusable Slotwise Mechanisms (RSM), a novel modular architecture comprising of a set of deep neural networks (representing reusable mechanisms) on top of slotwise representations established in prior work. Crucially, we take inspiration from a hypothesis in cognitive studies of consciousness, the Global Workspace Theory (Baars, 2005; 2017) (GWT), to introduce a *Central Contextual Information (CCI)*. CCI allows each reusable mechanism to leverage the information about *all* other slots, *through a bottleneck* for predicting the next state of a particular slot. CCI’s bottleneck acts as a middle ground, i.e., we do not predispose the interactions to be *only* pairwise, and nor do we allow for fully dense connections among slots. Moreover, the slots are updated in a sequential fashion within each time step, and the motivation for that is three-fold: a sequential update allows for symmetry breaking in selecting the mechanisms for slots, it better fits the sequential nature of the GWT, and it provides the transition function with autoregressive expressive power. We then show how RSM outperforms the state-of-the-art in a variety of next-step prediction tasks, both independent and identically distribution (iid) and out-of-distribution (OOD).

In summary, the presented work makes the following contributions:

1. RSM: A modular dynamics model comprising a set of reusable mechanisms which take as input slot representations through an attention bottleneck and sequential updates of slots.
2. RSM achieves state-of-the-art OOD performance com-

pared to baseline modular architectures in a range of long-term prediction tasks, both in terms of ranking metrics in the latent space, as well as in reconstruction.

3. Ablation studies show how CCI benefits the mechanism selection and the prediction task, compared with the baselines.

## 2. Proposed Method: RSM - Reusable Slotwise Mechanisms

### 2.1. RSM Overview

We propose RSM, a modular architecture comprising a set of  $M$  Multilayer Perceptrons (MLPs) as reusable mechanisms which act on top of slotwise representations to predict the changes in the latent state from  $t$  to  $t + 1$ . The key ingredient distinguishing RSM from its counterparts is the introduction of the Central Contextual Information (CCI) which effectively makes RSM flexible when dealing with environments of varying complexity of interactions among objects. Unlike prior works, we allow a sparse subset of the slots to propagate contextual information through a bottleneck for updating each slot. This permits reusable mechanisms to learn higher-order complex interaction in environments with events that can only be expressed as such, and also leaves room for mechanisms to choose less context when appropriate adaptively. CCI modulates the complexity of mechanisms and allows for the co-existence of mechanisms that need one or two slots, as well as those that require more information based on a larger subset of slots. This way, we avoid restricting the model to only modeling pairwise interactions (Goyal et al., 2020; 2021a), or very dense ones at the other extreme (Kipf et al., 2020; Ke et al., 2021). We find that this design choice results in significant improvements in OOD performance on a number of next-step prediction tasks.

An overview of the RSM pipeline is presented in figure 1(a). A given frame at time  $t$  is first passed through a Convolutional Neural Network (CNN) followed by an object encoder similar to (Kipf et al., 2020) to extract slot representations. Then within each time-step,  $t$  slot updates to  $t + 1$  will be computed *sequentially*. We opt for sequential updates because in addition to breaking symmetries when selecting mechanism for slots, they also allow for a more expressive transition function in the same way autoregressive models enable the expression of rich distributions, i.e., the updates from earlier slots can be taken into account when updating a particular slot. The sequential order is picked at random at the initial frame but is fixed for the whole rollout.

For the  $i$ -th slot  $s_t^i$  at  $t$ , the transition is computed via one of the reusable mechanisms. The responsible mechanism  $m_j$  is sampled from a categorical distribution over all  $M$  possibilities. This distribution is computed based on the CCI and the concatenation of the particular slot of interest and the action embedding  $a_t$ . The mechanism  $m_j$  takes as input the CCI along with  $s_t^i$ . As discussed earlier, CCI allows the propagation of information about all other slots through

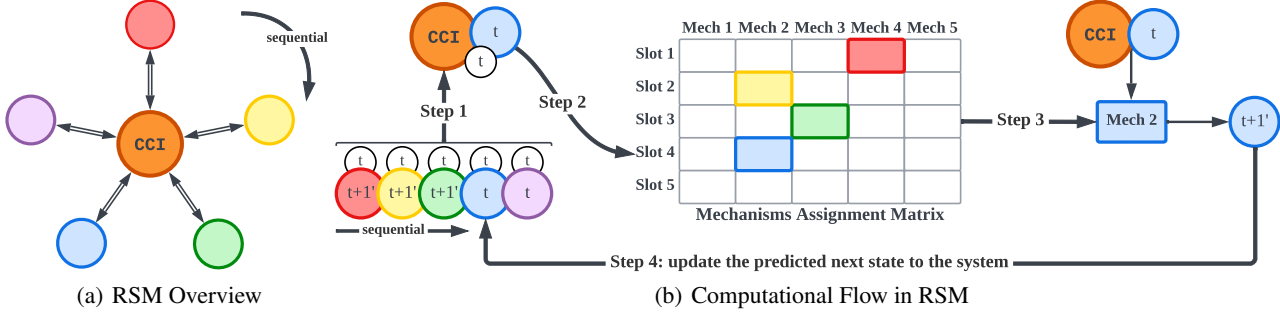


Figure 1: **RSM overview 1(a) and computational flow 1(b)**. RSM leverages Central Contextual Information (CCI), which is computed from all object slots and is used as context to select a mechanism for each slot, as well as a complementary input for predicting a slot’s next state. The small colored circles indicate slots, and white-filled circles represent the given action  $a_t$ . Slots are sequentially updated within a time step through a 4-step process: (1) Compute CCI from all slots (both updated ones and the rest) concatenated with the action  $a_t$  at time  $t$ , (2) select a mechanism (colored rectangles) for the slot based on CCI and the concatenation of the slot and  $a_t$  (3) predict the next state of the slot according to the dynamics specified by the selected mechanism, and (4) update the set of slots with the newly acquired prediction, and prepare to predict the next object’s update. The partially overlapped components indicate the concatenation operation of their respective representations.

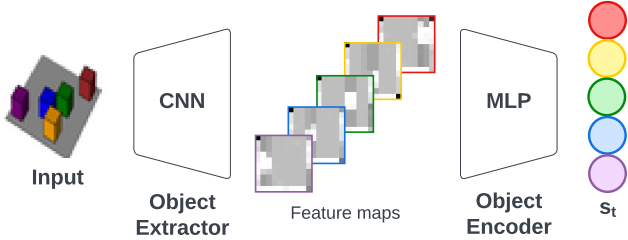


Figure 2: **Encoder Architecture** Slot representations are obtained by passing the input image to a CNN and feeding the output feature maps to another object encoder. This encoder directly follows that of (Kipf et al., 2020).

an attention bottleneck, and this is one key difference with similar modular works (Goyal et al., 2021b; 2020; 2021a; Ke et al., 2021). This process is updated until all such  $s_t^i$ ’s have been updated to their predicted values at  $t + 1$ .

## 2.2. Computational Flow in RSM

In this section, we describe the computational flow of RSM in more detail along a 4-step process that will be repeated for all slots within a time-step  $t$ , in a sequential manner, as illustrated in figure 1(b) and algorithm 1 in the Appendix. Given an input image  $x_t$ , we first feed it to a CNN object extractor followed by an MLP object encoder to obtain the set of  $N$  slot representations  $s_t^i \in \mathbb{R}^{d_s}$ . We use the same encoder as (Kipf et al., 2020), where feature maps act as object masks, and each object slot follows from an encoding of such feature maps. The following are the main components of the architecture:

1. **MultiheadAttention**( $\cdot$ ) :  $\mathbb{R}^{N \times (d_s + d_a)} \rightarrow \mathbb{R}^{d_s + d_a}$  that computes the CCI, denoted as  $cci \in \mathbb{R}^{d_{cci}}$ , from

all of the  $N$  slots concatenated by the given action embedding  $a_t \in \mathbb{R}^{d_a}$ . Keys, queries, and values all come from slots, so that the CCI is not affected by the order of feature maps and slot representations. Note that the encoder we use in this work follows that of (Kipf et al., 2020; Goyal et al., 2021a; Ke et al., 2021) and does not provide a *set* of slot representations as in (Locatello et al., 2020); therefore, we need to remove this order dependency through an attention mechanism.

2. The set of  $M$  reusable mechanisms  $\{g_1, \dots, g_M\}$  where  $g_i(\cdot) : \mathbb{R}^{d_{cci} + d_s} \rightarrow \mathbb{R}^{d_s}$  are represented by MLPs that are presumed to be independent and trained to implicitly specialize in explaining different transitions. Each such  $g_i(\cdot)$  takes as input one slot representation along with the CCI.
3.  $\psi(\cdot) : \mathbb{R}^{d_{cci} + d_s + d_a} \rightarrow \mathbb{R}^M$  that takes as input the CCI along with the concatenation of the action embedding  $a_t$  with the slot of interest  $s_t^i$ , computes a categorical distribution over the possible choices of mechanisms for  $s_t^i$ , and outputs a sample of that distribution to be used for updating  $s_t^i$ .

Given the  $N$  slots at time step  $t$ ,  $s_t = \{s_t^1, s_t^2, \dots, s_t^N\}$  and action  $a_t$ , RSM predicts the next state of slots at time step  $t + 1$  using the following 4-step process, which is sequentially applied to each of the slots. Suppose an ordering has been fixed over the slots for a rollout, and according to that ordering, for some  $n - 1 < N$  we have that  $n - 1$  slots  $s_t^1, \dots, s_t^{n-1}$  have been updated to their predicted values at  $t + 1$  and are denoted by  $s_{t+1}^i$ . Below we explain the process of computing the next state for  $s_t^n$ . (e.g. the blue slot in Figure 1(b)).

**Step 1. Compute the CCI:** We first concatenate  $a_t$  to each element of the sequence  $[s_{t+1}^1, s_{t+1}^2, \dots, s_t^n, \dots, s_t^N]$ . Afterward, a `MultiheadAttention()` (Vaswani et al., 2017) takes the previous sequence as input and transforms them via  $W_Q, W_K, W_V$  projections where queries, keys, and values all come from the elements of the sequence, and the output of the `MultiheadAttention` module is passed to a projection  $\phi(\cdot) : \mathbb{R}^{d_s+d_a} \rightarrow \mathbb{R}^{d_{cci}}$  that produces the central contextual information of size  $d_{cci}$ .

**Step 2. Select a mechanism for  $s_t^n$ :**  $\psi(\cdot)$  takes three arguments as inputs:  $cci$  which is the central contextual information from Step 1,  $s_t^n$ , and  $a_t$ , feeds them to an MLP which outputs the logits  $\log \pi_1, \dots, \pi_M$  of a categorical distribution over  $M$  possible choices of mechanisms. During training, mechanism selection is carried out by using a Gumbel – max layer (Maddison et al., 2016; Jang et al., 2017) on top of  $\psi$ 's outputs, and for inference at test time, we simply pick the argmax of  $\pi_i$ 's as the selected mechanism.

**Step 3. Predict the change of slot  $s_t^n$ :**  $\Delta s_t^{n,j}$  denotes the update that is predicted by the selected mechanism  $g_j$  and when applied to  $s_t^n$  gives its next state at  $t+1$ .  $\Delta s_t^{n,j}$  is computed by passing the concatenation of  $cci$  and  $s_t^n$  through  $g_j$ , i.e.,  $s_{t+1}^n = s_t^n + \Delta s_t^{n,j}$  where  $\Delta s_t^{n,j} = g_j([cci, s_t^n])$ .

**Step 4. Update and sync  $s_{t+1}^n$  with other slots:**  $s_{t+1}^n$  is then computed by adding  $\Delta s_t^{n,j} + s_t^n$  and replaces the value of  $s_t^n$  in the buffer of slots so we can similarly repeat this process for predicting the next state of  $s_{t+1}^n$ .

Following the above process repeats for all slots, we obtain the final output of the transition model  $s'_{t+1}$ , which results from the concatenation of  $N$  predicted slots  $s'_{t+1} = [s_{t+1}^1, \dots, s_{t+1}^N]$ .

### 3. Experiments

We evaluate and compare the performance of RSM and the baselines on the task of next-step prediction in a variety of environments ranging from Atari games to Physics environments and grid worlds. Additionally, we aim to provide evidence to support the following hypotheses, which inspire RSM's architectural design: (1) Reusable mechanisms of RSM are expected to specialize in modeling different interactions among slots as they compete for the explanation of each slot's transition dynamics. (2) RSM's mechanisms should benefit from the contextual information in modeling a wide array of interactions since the bottleneck can adaptively let varying amounts of information be fed to different mechanisms, providing a richer set of modules compared to the baselines with rigid priors over mechanism inputs. (3) By using slotwise representations along with the CCI that integrates information from all slots, RSM reduces information loss in the multi-step prediction of future states.

Below, we first provide a brief introduction to the experimental setup we used, as well as the baselines, followed

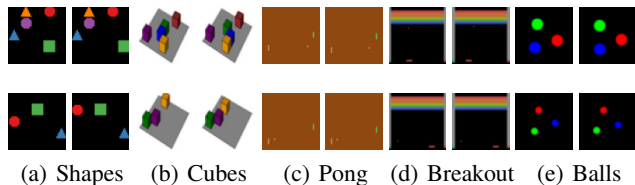


Figure 3: Examples of visual inputs used in the experiments. Each pair of images in either row shows two consecutive frames of an environment (five pairs in total per row). The top row illustrates the iid data, and the bottom row depicts the OOD data samples. Environment pairs from left to right: grid world (3(a), 3(b)), Atari games (3(c), 3(d)), and Physics simulation (3(e)).

by a comparison of their OOD generalization performance with RSM. We continue with exploring the specialization capabilities of RSM's mechanisms, followed by an investigation into the meaningfulness of RSM's learned slot representations compared to other methods. An ablation study concludes this section by aiming to shed light on the effectiveness of different architectural choices we have made.

#### 3.1. Environments

We demonstrate the effectiveness of RSM on five datasets from three categories: Atari games (Pong and Breakout), manipulation on a grid world (2D Shapes and 3D Cubes (Kipf et al., 2020)), and Physics simulation (Balls (Kipf et al., 2020)). At each time step, given an action and a single frame in the case of the grid world datasets, or two consecutive frames in the case of Atari games and Balls, the task is to predict the next state after the action is performed. We follow (Kipf et al., 2020; Liu et al., 2021) to generate the in-distribution (iid) and OOD datasets for each environment, as described in Appendix A.1. In addition, Figure 3 provides a visual comparison of the iid and OOD data.

#### 3.2. Baselines

We pick C-SWM (Kipf et al., 2020) as the most promising candidate among GNN-based methods for modeling transition dynamics. C-SWM uses the same inputs as RSM but uses shared node and edge update functions for modeling all transitions and predisposes the connections among slots to be dense. On the other hand, (Ke et al., 2021) propose an RL benchmark for evaluating structure learning and uses modular architecture where each slot can be updated by any of a given set of mechanisms; however, mechanisms take as input all other slots, i.e., dense connectivity is a feature of this method too. We refer to it as MBRL (Ke et al., 2021). Finally, NPS from (Goyal et al., 2021a) is the closest to our approach that has a set of reusable mechanisms used with slot representations, but compared to others, assumes all interactions to be pairwise, and thus, results in very sparse communications in contrast to the flexibility of RSM in that regard.



### 3.3. Experimental and Analytical Results

#### 3.3.1. NEXT STATE PREDICTION

Table 1 summarizes the comparison of the quantitative results between the proposed method and baselines on iid and OOD test sets. Overall, RSM achieves the highest scores in both iid and OOD settings in most of the cases and environments, which supports the hypothesis of improved generalization and robustness when learning the communication of slots in the latent space. We find that the baselines that do not use a modularized design for modeling the dynamics, such as C-SWM (Kipf et al., 2020), or do not utilize the general contextual information, such as (Ke et al., 2021; Goyal et al., 2021a), show a significant drop in OOD performance, especially in the Atari games and Physics simulation environments. RSM yields a smaller gap between the iid and OOD results and remains the most stable method for predicting 10 steps into the future in both iid and OOD setups. The main reason for this gap may be attributed to the sequential communication of slots through the attention bottleneck of the CCI within each prediction step. More specifically, the CCI in RSM facilitates the effectiveness of communications among slots by making it easier for a slot to observe the changes of others before predicting its update. This would reduce the small prediction errors from each slot that accumulate and corrupt the prediction (see the analysis in Section E). Consequently, all of the baselines that do not allow observing the changes of other slots fare poorly on 10-step rolling-out predictions.

#### 3.3.2. MECHANISMS ARE NOT INTERCHANGEABLE, AND A PROPER ASSIGNMENT IS NECESSARY

Figure 4 supports our hypothesis that mechanisms tend to specialize in modeling non-overlapping transitions. We can see that if we ignore our mechanism selection procedure and assign a mechanism to each slot at random, the performance drops significantly as the rollout continues further in time, supporting the hypothesis that mechanisms are not interchangeable and that the mechanism selection is an essential element of RSM’s high performance.

#### 3.4. Mechanisms specialize in modeling different transitions

To continue clarifying hypothesis 1 and start analyzing hypothesis 2, in Figure 5, we study the role of each mechanism in RSM. The RSM reconstruction results are presented in the second row, whereas, in the last five rows, a single mechanism is assigned to all slots for all of the 10 roll-out prediction steps. The analysis shows that RSM not only produces a reasonable reconstruction compared to the ground-truth frame but also encourages the mechanisms to distinguish themselves in the roles they take. In this sample, we have the 5 slots corresponding to: 1: red round, 2: blue triangle, 3: green square, 4: purple round, and 5: yellow triangle.

Looking deeper into the reconstruction result, RSM takes advantage of the CCI to assign a suitable mechanism for

each slot in all scenarios. More specifically, there are three scenarios of objects in 2D Shapes: (1) *Allowed to move* as in steps  $0 \rightarrow 1$  and  $1 \rightarrow 2$ ; (2) *Blocked by the wall* as in steps  $2 \rightarrow 3$ ,  $3 \rightarrow 4$ ; and (3) *Blocked by an object* that occupies the desired destination as in step  $4 \rightarrow 5$ . RSM predicts the movement (to the right) of the yellow triangle accurately in the first case and predicts the *zero* changes of slots and preserves the system status due to no movement happening in cases 2 and 3.

From the visualization, we find that the mechanisms specialize with respect to the action: Mechanism 1: RIGHT, Mechanism 2: UP, Mechanism 3: LEFT, Mechanism 4: *DO NOT MOVE*, and Mechanism 5: DOWN. However, for the same action, RSM considers the particular situation and reacts differently. For instance, with the same action UP given in step 1 (green bounding box) on the green rectangle and step 3 (red bounding box) on the red round, RSM recognizes the situations that the object is allowed to move and blocked by the upper wall, respectively, then applies the movement at step 1 while not modifying objects at step 3 and generating the correct reconstruction in both cases. We can see a similar example in the row of mechanism 2 at step  $3 \rightarrow 4$  (cyan bounding box) when the green object does not move UP but remains at the same position since it is blocked by the red object.

NPS enables a null rule to produce *zero* change of the primary slot. RSM achieves the same without any artificially defined procedure: it implicitly recognizes the possibility of *zero* modification of a slot, then assigns the procedure of *DO NOT MOVE* to a particular mechanism, as demonstrated by mechanism 4 in Figure 5.

Appendix C provides the visualization of the entire 10 roll-out steps of the 2D Shapes and Balls environments.

#### 3.4.1. THE ABILITY TO DECOMPOSE THE VISUAL FRAME INTO SLOTS

We conduct a qualitative comparison to clarify hypothesis 3 about the effectiveness of RSM in the slot-centric representation learning task. In Figure 7, we illustrate a comparison of the extracted feature maps with a size of  $10 \times 10$ , which are constructed by the Encoder model. Afterward, in Figure 8, we illustrate the reconstructed slots and frame with a size of  $3 \times 50 \times 50$ , which are acquired by the Decoder model that receives the input as the predicted next state. We find that RSM decomposes objects in the input frame into separated slots and keeps each object in the same slot until they are decoded. In contrast, the baselines do not capture all objects, they produce noised feature maps (MBRL), or put the same object in two slots and identify two objects in another slot (NPS).

We observe that the combination of the CCI with the sequential updates that encourage slots to observe the modification of each other benefits from recognizing the overlap of objects. More specifically, RSM only generates a part of the object in case that object is covered by another one (*e.g.* the

Table 1: **Comparison of the prediction in latent space** between the proposed RSM and the baselines in both iid and OOD test sets. The mean and standard error of ranks over 30 seeds are reported. Larger scores indicate better predictions. The best scores are in **bold**, with RSM winning much more often than any of the baselines, and always winning OOD.

		iid			OOD		
		<i>1 step</i>	<i>5 steps</i>	<i>10 steps</i>	<i>1 step</i>	<i>5 steps</i>	<i>10 steps</i>
Shapes	C-SWM	<b>100.0</b> $\pm$ 0.0	<b>100.0</b> $\pm$ 0.0	<b>100.0</b> $\pm$ 0.0	93.0 $\pm$ 0.6	81.3 $\pm$ 0.7	72.1 $\pm$ 0.8
	MBRL	<b>100.0</b> $\pm$ 0.0	99.8 $\pm$ 0.0	98.0 $\pm$ 0.1	95.9 $\pm$ 0.2	85.3 $\pm$ 0.3	69.7 $\pm$ 0.8
	NPS	<b>100.0</b> $\pm$ 0.0	99.7 $\pm$ 0.1	97.0 $\pm$ 0.3	95.2 $\pm$ 0.2	81.7 $\pm$ 0.6	65.5 $\pm$ 0.5
	RSM (Ours)	<b>100.0</b> $\pm$ 0.0	99.9 $\pm$ 0.0	97.9 $\pm$ 0.1	<b>96.8</b> $\pm$ 0.0	<b>91.1</b> $\pm$ 0.2	<b>80.9</b> $\pm$ 0.3
Cubes	C-SWM	<b>100.0</b> $\pm$ 0.2	<b>99.6</b> $\pm$ 0.0	<b>98.2</b> $\pm$ 0.5	78.1 $\pm$ 5.5	52.7 $\pm$ 8.7	40.6 $\pm$ 8.3
	MBRL	99.8 $\pm$ 0.1	99.1 $\pm$ 0.2	96.5 $\pm$ 0.4	95.2 $\pm$ 0.3	85.6 $\pm$ 1.3	71.3 $\pm$ 1.9
	NPS	99.8 $\pm$ 0.2	99.1 $\pm$ 0.6	96.6 $\pm$ 1.6	94.4 $\pm$ 0.7	75.4 $\pm$ 4.2	63.2 $\pm$ 5.4
	RSM (Ours)	99.8 $\pm$ 0.0	99.2 $\pm$ 0.6	93.9 $\pm$ 1.5	<b>97.5</b> $\pm$ 0.2	<b>89.6</b> $\pm$ 0.9	<b>77.5</b> $\pm$ 1.5
Breakout	C-SWM	65.6 $\pm$ 4.1	36.7 $\pm$ 3.7	21.8 $\pm$ 2.2	27.0 $\pm$ 3.8	5.4 $\pm$ 1.0	2.8 $\pm$ 0.7
	MBRL	64.7 $\pm$ 1.2	37.4 $\pm$ 1.8	14.9 $\pm$ 2.1	30.7 $\pm$ 4.0	4.6 $\pm$ 0.3	2.1 $\pm$ 0.3
	NPS	68.0 $\pm$ 0.3	44.5 $\pm$ 1.1	<b>27.2</b> $\pm$ 1.5	28.1 $\pm$ 1.5	4.9 $\pm$ 2.0	3.9 $\pm$ 1.0
	RSM (Ours)	<b>73.3</b> $\pm$ 1.0	<b>46.6</b> $\pm$ 1.7	<b>27.2</b> $\pm$ 2.0	<b>39.8</b> $\pm$ 0.1	<b>19.1</b> $\pm$ 0.4	<b>10.1</b> $\pm$ 1.2
Pong	C-SWM	44.2 $\pm$ 4.9	21.4 $\pm$ 1.9	15.2 $\pm$ 1.7	10.8 $\pm$ 2.4	2.1 $\pm$ 0.5	2.0 $\pm$ 0.4
	MBRL	50.3 $\pm$ 2.0	23.9 $\pm$ 1.5	16.8 $\pm$ 2.1	15.9 $\pm$ 2.0	2.5 $\pm$ 0.3	1.7 $\pm$ 0.3
	NPS	52.0 $\pm$ 5.0	24.2 $\pm$ 1.6	15.4 $\pm$ 2.2	14.6 $\pm$ 3.2	2.0 $\pm$ 0.4	0.8 $\pm$ 0.4
	RSM (Ours)	<b>53.9</b> $\pm$ 1.5	<b>30.6</b> $\pm$ 1.0	<b>23.5</b> $\pm$ 0.7	<b>41.6</b> $\pm$ 0.8	<b>24.8</b> $\pm$ 1.6	<b>18.6</b> $\pm$ 2.1
Balls	C-SWM	99.7 $\pm$ 0.1	86.6 $\pm$ 4.9	64.9 $\pm$ 8.8	76.8 $\pm$ 5.5	11.6 $\pm$ 2.8	2.6 $\pm$ 0.8
	MBRL	99.8 $\pm$ 0.1	89.7 $\pm$ 4.5	68.1 $\pm$ 6.0	74.8 $\pm$ 4.8	9.9 $\pm$ 2.5	2.6 $\pm$ 0.8
	NPS	<b>100.0</b> $\pm$ 0.0	89.5 $\pm$ 1.9	<b>73.2</b> $\pm$ 3.3	78.2 $\pm$ 0.4	11.1 $\pm$ 3.7	9.3 $\pm$ 3.8
	RSM (Ours)	99.8 $\pm$ 0.0	<b>92.9</b> $\pm$ 1.8	72.6 $\pm$ 4.5	<b>84.3</b> $\pm$ 1.9	<b>28.3</b> $\pm$ 4.2	<b>19.6</b> $\pm$ 2.4

green and blue cubes in slot 2 and slot 4 are partially covered by the yellow cube). On the other hand, the reconstructed frames by the baselines overlook the information of the objects’ visible order, generating overlapped objects in some cases (*e.g.* the green, blue, and yellow cubes in MBRL overlapped to each other). We further discuss this conclusion in Appendix D and E.

### 3.5. Ablation Studies

We conduct ablation studies to better understand the role of CCI in RSM, by trying to reduce the effect of the CCI in different places of the original design of RSM. We denote “RSM ab  $ij$ ”, with  $i, j \in \{0, 1\}$ , for the ablation of reducing the usage of CCI in different places from the original RSM algorithm. More specifically,  $i$  is equal to 1 if the CCI is used as the input of the mechanism selection at step 2, 0 otherwise. A similar concept for  $j$  indicates the usage of CCI in the mechanism’s input at step 3. Following the notation above, we have this list of ablations: “RSM ab 01”, “RSM ab 10”, and “RSM ab 00”. In addition, we design the “RSM ab par” making parallel instead of sequential updates, which reduces the effect of the CCI in information integration among slots. Finally, “MLP-CCI” replaces the MultiheadAttention by an MLP architecture.

“RSM ab 01” is the main ablation that breaks the original

idea, making RSM similar to NPS, which does not have the information extracted from all the slots in selecting the mechanism.

The ablation studies results are visualized in Figure 6. Overall, the ablation results confirm the proposed hypotheses to explain the advantage of RSM, exposing the dominance of the original design of RSM over the ablations. In particular, the absence of the CCI in RSM ab 01 causes a drastic drop in H@1, especially for the OOD results (-10% in grid world, -15% in Atari, and -20% in Balls at step 10) compared with the regular RSM.

For more results and analyses on the ablation studies, we refer the reader to Appendix E.

## 4. Related Works

In this paper, we proposed a modular architecture for learning slotwise interactions based on representations that are jointly learned end-to-end. In the following, we provide an overview of related works on learning slot-based representations, as well as learning object dynamics.

### Unsupervised learning of slot-centric representations.

To decompose a scene into meaningful sub-parts, there have been lots of recent works on unsupervised learning of object-centric representations from static images (Greff

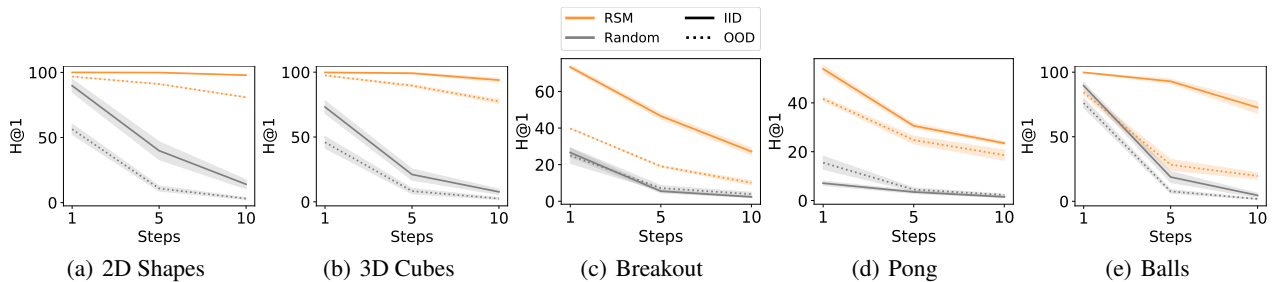


Figure 4: **Input-based one-hot mechanism selection is important for model performance.** To understand the contribution of mechanism selection to model performance in the visual task, RSM is compared with a modified version in which a random mechanism is assigned for the prediction at each time step. The results suggest that the mechanism picking learned by RSM has a significant contribution to performance on both in-distribution and out-of-distribution test sets.

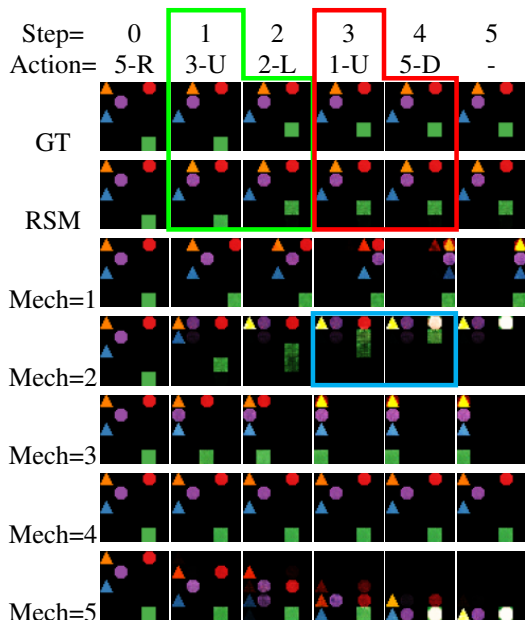


Figure 5: Observation of mechanisms assignment and mechanisms performance during 5 rolling out steps in 2D Shapes environment. GT stands for ground-truth images. The last 5 rows represent the reconstruction with a single mechanism assigned for all slots. See text for analysis.

et al., 2017; Locatello et al., 2020), or videos (Pervez et al., 2022; Kipf et al., 2022; Elsayed et al., 2022), as well as theory results on the identifiability of such representations (Mansouri et al., 2022; Ahuja et al., 2022).

**Learning object dynamics.** R-NEM (van Steenkiste et al., 2018) was the first fully unsupervised method capable of modeling dynamics through a learned object-centric latent space. Other attempts include RIMs (Goyal et al., 2021b), SCOFF (Goyal et al., 2020), and the closest to our work which is NPS (Goyal et al., 2021a). The works along this line can be divided into two classes. One class uses GNNs to model pairwise interactions (Kipf et al., 2020; Watters et al., 2017; van Steenkiste et al., 2018), and the other class uses a

set of rules or mechanisms represented by deep neural nets to model the dynamics (Goyal et al., 2021b; 2020; 2021a). Our work differs from the former group in two important ways similar to (Goyal et al., 2021a); namely, we do not employ GNNs as the machinery to model interactions, because such design assumes interactions to be dense, which is not a realistic inductive bias in many environments. More importantly, there is no potential to learn a *set* of simple rules that can be recombined and re-purposed to deal with novel scenarios. Instead, a GNN limits the agent to compressing an abundance of information via node and edge updates which are indeed shared among all slots, whereas we want to learn a set of simple and reusable mechanisms to *choose* from, based on the content and context of each slot. We include C-SWM (Kipf et al., 2020) as a representative baseline of GNN-based methods and turn most of our focus to modular architectures for learning the dynamics.

**Modular dynamics models.** Among earlier works on modular neural networks, RIMs (Goyal et al., 2021b) is the first notable approach that studies modularity for learning the dynamics and long-term dependencies in non-stationary settings. They propose a set of recurrent independent mechanisms (RIMs) for capturing the transition dynamics; however, these RIMs conflate the notions of object and mechanism, i.e., each RIM is responsible for representing a part of the visual input, as well as predicting its evolution. SCOFF (Goyal et al., 2020) addresses this issue by leveraging the notions of *object files* (OF) and *schemata* referring to now separated mechanisms and object representations. Although SCOFF achieves reasonable performance on some tasks, we show its difficulty in generalizing OOD. The main differences between RSM and SCOFF are that 1) a SCOFF schema can admit only one OF at a time, whereas RSM allows more than two slots to be input to any of its reusable mechanisms via an attention bottleneck, and 2) SCOFF, similar to RIMs uses a sparse communication among the OFs themselves to handle rare events that involve more than one object, whereas RSM is inspired by the assumption that such events should in principle activate one of the reusable

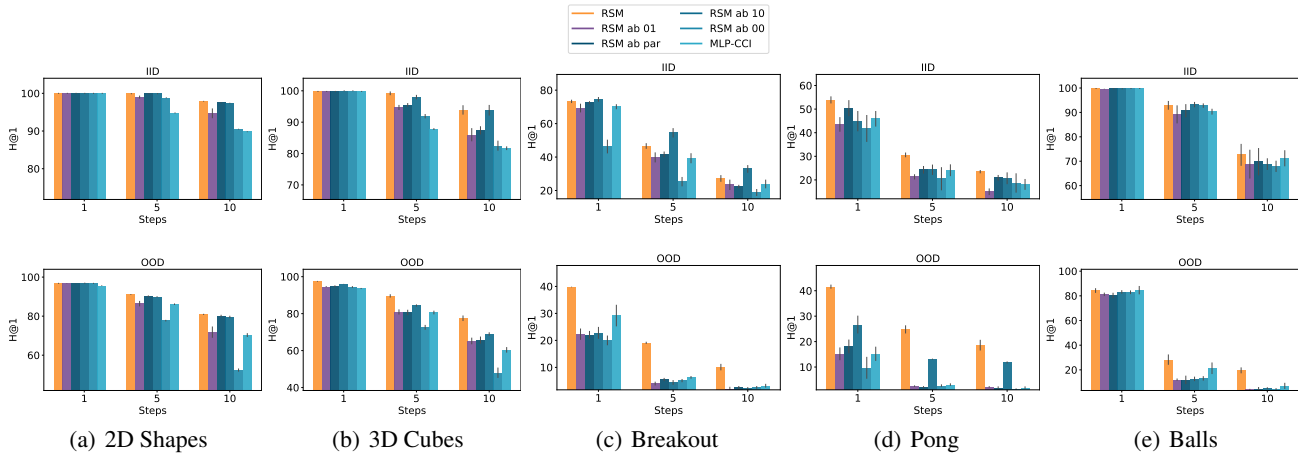


Figure 6: **Ablation studies** to clarify the importance of the CCI in mechanisms selection. The original design of RSM, which includes the usage of CCI in mechanism assignment in a sequential manner, demonstrates the strongest results in all environments compared to the ablations.

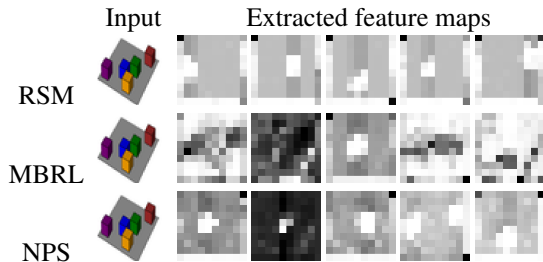


Figure 7: Slotwise representation learned by RSM shows better separation among objects. Comparison of extracted feature maps from a scene in the 3D Cubes environment suggests that different objects (3D colored blocks in the input figures) are better separated in representations learned by RSM.

mechanisms which can deal with such scenarios, with the help of CCI. Similar to SCOFF (Goyal et al., 2020), NPS (Goyal et al., 2021a) bakes in the assumption of sparse interactions into its modular architecture instead of requiring slots or OFs to communicate sparsely, i.e., *production rules*, which are counterparts to schemata in SCOFF or reusable mechanisms in RSM, can now take as input one primary slot as well as a contextual slot to handle rare events that involve more than one object. Lastly, (Ke et al., 2021) propose a new benchmark for evaluating the capabilities of different models for causal discovery. They also propose a modular architecture that is similar to GNN-based methods in that object interactions are dense (in fact, fully connected), but closer to modular designs in that each object is assigned a separate mechanism.

### 5. Conclusion

In this study, we developed RSM, a modular dynamics model for visual prediction tasks. RSM comprises a set

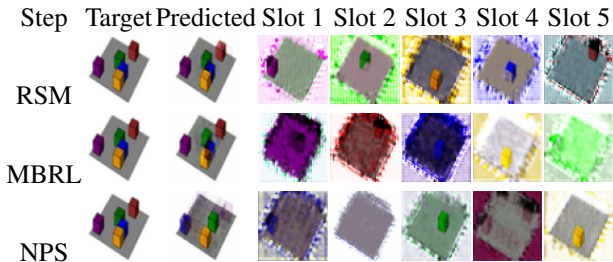


Figure 8: Comparison of the decoded slots at step 5 in the 3D Cubes environment. RSM generates the most meaningful slots and frame reconstruction compared to other models with modular design

of reusable mechanisms which take as input slot representations through a global attention bottleneck (the Central Contextual Information, CCI) and sequential updates of the slots. Through empirical experiments and analysis, we show that RSM has advantages over other methods with similar inductive biases, especially in terms of OOD generalization, long-term future frame prediction, separating different mechanisms, and taking contextual information in the environment into consideration. Through behavior analysis and an ablation study, our results suggest the importance of CCI, which integrates and coordinates knowledge from different slots for both mechanism picking and slot updates. Future work should involve intricate stochastic attention for information integration that is more consistent with higher-level cognition, mechanisms that are able to cope with a large number of slots and objects, as well as uncertainty or confidence quantification in the predictions.



## References

- Ahuja, K., Hartford, J., and Bengio, Y. Weakly supervised representation learning with sparse perturbations. *arXiv preprint arXiv: Arxiv-2206.01101*, 2022.
- Baars, B. J. Global workspace theory of consciousness: toward a cognitive neuroscience of human experience. In Laureys, S. (ed.), *The Boundaries of Consciousness: Neurobiology and Neuropathology*, volume 150 of *Progress in Brain Research*, pp. 45–53. Elsevier, 2005. doi: [https://doi.org/10.1016/S0079-6123\(05\)50004-9](https://doi.org/10.1016/S0079-6123(05)50004-9). URL <https://www.sciencedirect.com/science/article/pii/S0079612305500049>.
- Baars, B. J. *The Global Workspace Theory of Consciousness*. John Wiley & Sons, Ltd, 2017. ISBN 9781119132363.
- Elsayed, G. F., Mahendran, A., van Steenkiste, S., Greff, K., Mozer, M. C., and Kipf, T. SAVi++: Towards end-to-end object-centric learning from real-world videos. 2022.
- Fernando, C., Banarse, D., Blundell, C., Zwols, Y., Ha, D., Rusu, A. A., Pritzel, A., and Wierstra, D. Pathnet: Evolution channels gradient descent in super neural networks. *CoRR*, 2017.
- Goyal, A. and Bengio, Y. Inductive biases for deep learning of higher-level cognition. *CoRR*, abs/2011.15091, 2020.
- Goyal, A., Lamb, A., Gampa, P., Beaudoin, P., Levine, S., Blundell, C., Bengio, Y., and Mozer, M. Object files and schemata: Factorizing declarative and procedural knowledge in dynamical systems. *arXiv preprint arXiv:2006.16225*, 2020.
- Goyal, A., Didolkar, A., Ke, N. R., Blundell, C., Beaudoin, P., Heess, N., Mozer, M., and Bengio, Y. Neural production systems. *CoRR*, abs/2103.01937, 2021a.
- Goyal, A., Lamb, A., Hoffmann, J., Sodhani, S., Levine, S., Bengio, Y., and Schölkopf, B. Recurrent independent mechanisms. 2021b.
- Graves, A., Wayne, G., and Danihelka, I. Neural Turing machines. *CoRR*, abs/1410.5401, 2014.
- Greff, K., Van Steenkiste, S., and Schmidhuber, J. Neural expectation maximization. *Advances in Neural Information Processing Systems*, 2017.
- Henaff, M., Weston, J., Szlam, A., Bordes, A., and LeCun, Y. Tracking the world state with recurrent entity networks. 2017.
- Jang, E., Gu, S., and Poole, B. Categorical reparameterization with gumbel-softmax. In *5th International Conference on Learning Representations, ICLR 2017, Toulon, France, April 24-26, 2017, Conference Track Proceedings*. OpenReview.net, 2017. URL <https://openreview.net/forum?id=rkE3y85ee>.
- Ke, N. R., Didolkar, A., Mittal, S., Goyal, A., Lajoie, G., Bauer, S., Rezende, D., Bengio, Y., Mozer, M., and Pal, C. Systematic evaluation of causal discovery in visual model based reinforcement learning. 2021.
- Kingma, D. P. and Ba, J. Adam: A method for stochastic optimization. In Bengio, Y. and LeCun, Y. (eds.), *3rd International Conference on Learning Representations, ICLR 2015, San Diego, CA, USA, May 7-9, 2015, Conference Track Proceedings*, 2015. URL <http://arxiv.org/abs/1412.6980>.
- Kipf, T., van der Pol, E., and Welling, M. Contrastive learning of structured world models. In *International Conference on Learning Representations*, 2020.
- Kipf, T., Elsayed, G. F., Mahendran, A., Stone, A., Sabour, S., Heigold, G., Jonschkowski, R., Dosovitskiy, A., and Greff, K. Conditional object-centric learning from video. *ICLR*, 2022.
- Li, S., Li, W., Cook, C., Zhu, C., and Gao, Y. Independently recurrent neural network (indrnn): Building a longer and deeper rnn. 2018.
- Liu, D., Lamb, A. M., Kawaguchi, K., ALIAS PARTH GOYAL, A. G., Sun, C., Mozer, M. C., and Bengio, Y. Discrete-valued neural communication. In *Advances in Neural Information Processing Systems*, 2021.
- Liu, D., Shah, V., Boussif, O., Meo, C., Goyal, A., Shu, T., Mozer, M. C., Heess, N. M. O., and Bengio, Y. Stateful active facilitator: Coordination and environmental heterogeneity in cooperative multi-agent reinforcement learning. *ArXiv*, abs/2210.03022, 2022.
- Locatello, F., Weissenborn, D., Unterthiner, T., Mahendran, A., Heigold, G., Uszkoreit, J., Dosovitskiy, A., and Kipf, T. Object-centric learning with slot attention. *NIPS'20*, 2020.
- Madan, K., Ke, N. R., Goyal, A., Schölkopf, B., and Bengio, Y. Fast and slow learning of recurrent independent mechanisms. 2021. URL <https://arxiv.org/abs/2105.08710>.
- Maddison, C. J., Mnih, A., and Teh, Y. The concrete distribution: A continuous relaxation of discrete random variables. *International Conference On Learning Representations*, 2016.
- Mansouri, A., Hartford, J., Ahuja, K., and Bengio, Y. Object-centric causal representation learning. *NeurIPS Workshop on Symmetry and Geometry*, 2022.
- Pervez, A., Lippe, P., and Gavves, E. Differentiable mathematical programming for object-centric representation learning. *arXiv preprint arXiv: Arxiv-2210.02159*, 2022.

- Rosenbaum, C., Cases, I., Riemer, M., and Klinger, T. Routing networks and the challenges of modular and compositional computation. *CoRR*, abs/1904.12774, 2019.
- Santoro, A., Faulkner, R., Raposo, D., Rae, J., Chrzanowski, M., Weber, T., Wierstra, D., Vinyals, O., Pascanu, R., and Lillicrap, T. Relational recurrent neural networks, 2018. URL <https://arxiv.org/abs/1806.01822>.
- Shazeer, N., Mirhoseini, A., Maziarz, K., Davis, A., Le, Q. V., Hinton, G. E., and Dean, J. Outrageously large neural networks: The sparsely-gated mixture-of-experts layer. *CoRR*, abs/1701.06538, 2017.
- van Steenkiste, S., Chang, M., Greff, K., and Schmidhuber, J. Relational neural expectation maximization: Unsupervised discovery of objects and their interactions. *International Conference On Learning Representations*, 2018.
- Vaswani, A., Shazeer, N., Parmar, N., Uszkoreit, J., Jones, L., Gomez, A. N., Kaiser, Ł., and Polosukhin, I. Attention is all you need. *Advances in neural information processing systems*, 30, 2017.
- Watters, N., Tacchetti, A., Weber, T., Pascanu, R., Battaglia, P., and Zoran, D. Visual interaction networks. *arXiv preprint arXiv: Arxiv-1706.01433*, 2017.
- Wu, Z., Dvornik, N., Greff, K., Xi, J., Kipf, T., and Garg, A. Slotformer: Long-term dynamic modeling in object-centric models. 2022.

---

**Algorithm 1** Reusable Slotwise Mechanisms

---

**Input:**  $s_t = [s_t^1, s_t^2, \dots, s_t^N]$ : input slots at time  $t$ ,  $a_t$ : input action at time  $t$ ,  $\tilde{s}_t$ : the action-augmented state  $[s_t, a_t]$

**Output:**  $s_{t+1}^i$ : predicted slots at time  $t + 1$

$N$ : number of slots

$M$ : number of mechanisms

$d_s$ : slot dimension

$d_a$ : action dimension

$d_{cci}$ : central contextual information dimension

$\mathbf{W}_q, \mathbf{W}_k, \mathbf{W}_v : \mathbb{R}^{d_s+d_a} \rightarrow \mathbb{R}^{d_s+d_a}$  denote query, key, and value projection layers transforming the concatenation of  $[s_t, a_t]$  in the attention mechanism.

**MultiheadAttention** $(\cdot) : \mathbb{R}^{N \times (d_s+d_a)} \rightarrow \mathbb{R}^{d_s+d_a}$ : apply self-attention on the concatenation of  $[s_t, a_t]$

$\phi(\cdot) : \mathbb{R}^{d_s+d_a} \rightarrow \mathbb{R}^{d_{cci}}$  computes the central contextual information by passing the outputs of the **MultiheadAttention** $(\cdot)$  through a nonlinear transformation (MLP).

$\psi(\cdot) : \mathbb{R}^{d_{cci}+d_s+d_a} \rightarrow \mathbb{R}^M$  computes the unnormalized probability of selecting a mechanism from  $M$  possible choices by taking  $[cci, s_t^i, a_t]$  as input and feeding that to an MLP.

Set of  $M$  mechanisms  $g_j(\cdot) : \mathbb{R}^{d_{cci}+d_s} \rightarrow \mathbb{R}^{d_s}, j \in \{1 \dots M\}$ : predict the changes of each slot  $s_t^i$  based on  $[cci, s_t^i]$ . These are also realized with MLPs.

**for each**  $s_t^i$  in  $s_t$  with  $i \in 1 \dots N$  **do**

*Step 1: Compute the central context*

$\tilde{s}_t = \text{concat}(s_t, a_t)$

$cci = \phi(\text{MultiheadAttention}(\mathbf{W}_q(\tilde{s}_t), \mathbf{W}_k(\tilde{s}_t), \mathbf{W}_v(\tilde{s}_t)))$

*Step 2: Select a mechanism for slot  $s_t^i$*

$p = \text{Gumbel}(\psi(\text{concat}(cci, s_t^i, a_t^i)))$

*Step 3: Apply the selected mechanism to slot  $s_t^i$ , note that  $p$  is one-hot.*

$\Delta s_t^{i,j} = g_j(\text{concat}(cci, s_t^i)) * p^j \quad \forall j \in \{1, \dots, M\}$

$\Delta s_t^i = \sum_{j=1}^M \Delta s_t^{i,j}$

*Step 4: Update the slots buffer with the new value of  $s_t^{i+1}$*

$s_{t+1}^i = s_t^i + \Delta s_t^i$

**end for**

---

## A. Experiment Details

### A.1. Environment details

#### A.1.1. PREDICT THE NEXT STEPS IN ATARI GAMES

We explore the Atari 2600 environments, which are commonly used in (Kipf et al., 2020; Goyal et al., 2021b; Liu et al., 2021). The challenge of this kind of environment is that multiple factors cause the movements in two consecutive time steps; however, the given action has only affected the movement of a single object. For instance, there are 3 factors in Pong, which are (1) the ball follows physics rules to keep moving towards or collide with the walls or the two paddles, (2) the green paddle is controlled by the given action, (3) the white paddle that follows the movement of the ball.

Following (Kipf et al., 2020; Liu et al., 2021) in the OOD test set generation, we set up the variable warmstart that designates the number of frames to be discarded from the beginning before recording the game. Afterward, we use the same warmstart to produce the train, evaluation, and the iid test set while using another value of warmstart to generate the OOD test set.

#### A.1.2. MANIPULATIONS IN GRID WORLD

This dataset contains a number of objects placed in a  $5 \times 5$  grid. At each time step, given a single frame and an action that specifies one object and one manipulation from UP, RIGHT, DOWN, and LEFT. The challenge of this task is to consider the feasibility of the given action and predict the next frame. For instance, moving an object to LEFT is executable if there is no object occupied on the left of that object; otherwise, the frame is not changed.

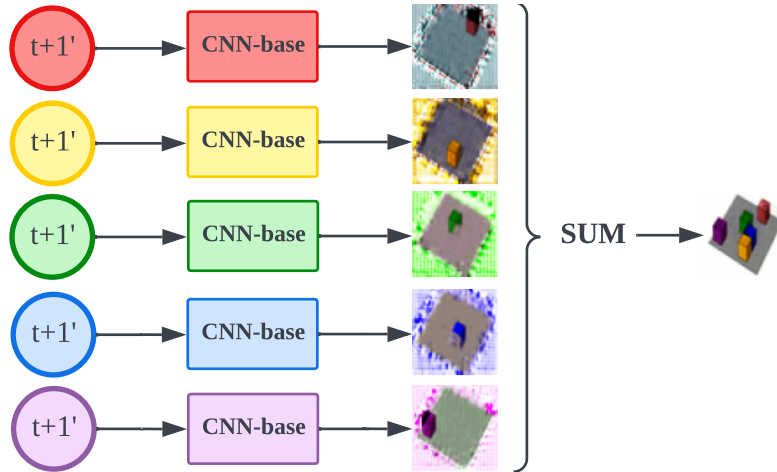


Figure 9: **Decoder architecture** contains a list of  $N$  CNN-based decoders corresponding to  $N$  slots that share the same structure. The frame reconstruction is obtained by the sum of  $N$  slot reconstructions.

For both 2D Shapes and 3D Cubes, we generate 5 objects for iid sets and 3 objects for the OOD test set.

### A.1.3. MOVEMENTS IN PHYSICS SIMULATION

We investigate the physic simulation environment introduced by (Kipf et al., 2020), containing three balls moving by the same and unchanged velocities in a 2D plane. Different from the rest of the environments in this study, the environment Balls is not governed by any given action. The challenge of this task is to recognize the latent velocities at the beginning time and generate the next step with the constant movement of objects.

The ball radius equals 4 in the training set and iid test set, while the ball radius is set to 5 in the evaluation set and 3 for the OOD test set.

## A.2. Encoder and Decoder architecture

### A.2.1. ENCODER ARCHITECTURE

In this work, we follow the encoder architecture from baselines (Kipf et al., 2020; Ke et al., 2021; Liu et al., 2021) that contains 2 components:

- Object Extractor: CNN layers that extract the visual input to  $N$  feature maps.
- Object Encoder: MLP layers to encoding feature maps to vector space, *i.e.* the object slots.

Afterward, an Encoder model consists of a single Object Extractor and a single Object Encoder.

### A.2.2. DECODER ARCHITECTURE

We construct a new architecture for the Decoder working on slot-based visual prediction tasks. We propose the Slot Decoder that decodes a single slot to frame.

$$s_{t+1}^m \in \mathbb{R}^{d_s} \rightarrow \text{Slot Decoder} \rightarrow \text{slot reconstruction} \in \mathbb{R}^{3 \times 50 \times 50}$$

Then, a Decoder model consists of  $N$  Slot Decoders that share the same architecture but different weights.

Figure 9 provides the overview of the proposed decoder architecture. Specifically, each slot in the latent space is passed through a corresponding Slot Decoder model to produce an RGB slot reconstruction. Finally, the frame reconstruction is obtained by the sum of  $N$  slots reconstruction with a size of  $3 \times 50 \times 50$ .

In this study, we use the described architecture for the proposed method and baselines.

## A.3. Loss Functions

### A.3.1. CONTRASTIVE LOSS DURING TRAINING THE ENCODER AND TRANSITION MODEL

In this study, we follow the same Contrastive loss setup as (Kipf et al., 2020), which is also used in all of the baselines. In this setup, we use the prediction result of the model to form the positive hypothesis, whereas, we sample random input states



in the same batch to form the negative hypothesis.

Mathematically, the Contrastive loss function can be described as follow:

$$\begin{aligned}
 H &= \text{MSE}(s'_{t+1}, s_{t+1}) \\
 \tilde{H} &= \text{MSE}(\tilde{s}_{t+1}, s_{t+1}) \\
 \text{Contrastive Loss} : \mathcal{L} &= H + \max(0, \gamma - \tilde{H})
 \end{aligned}
 \tag{1}$$

where  $s_{t+1}$  denotes the abstract target state obtained by passing the target observation ( $x_{t+1}$ ) through *encoder*,  $s'_{t+1}$  represent the abstract next state output by the transition model, and  $\tilde{s}_{t+1}$  indicates the random abstract state in the training batch of data.  $\gamma$  is a hyper-parameter which is set to 1 by following (Kipf et al., 2020).

### A.3.2. BINARY CROSS ENTROPY IN TRAINING THE DECODER

We consider two BCE loss terms in training Decoder,  $\mathcal{L}_1$  and  $\mathcal{L}_2$ , as mathematically described in Equation (3). More specifically,  $\mathcal{L}_1$  is computed by passing  $s_t$  through Decoder to achieve  $x'_t$  which is expected to close to  $x_t$ .  $\mathcal{L}_1$  follow the same procedure that passing the output of transition model, the abstract states  $s'_{t+1}$ , to achieve the prediction of next frames,  $x'_{t+1}$ , that is desired to close to the observation at time  $t + 1$ , denoted as  $x_{t+1}$ . Then, the final BCE loss for the Decoder training is formularized as in Equation (3).

$$\begin{aligned}
 x'_t &= \text{Decoder}(s_t) \\
 x'_{t+1} &= \text{Decoder}(s'_{t+1})
 \end{aligned}
 \tag{2}$$

$$\begin{aligned}
 \mathcal{L}_1 &= \text{BCE}(x'_t, x_t) \\
 \mathcal{L}_2 &= \text{BCE}(x'_{t+1}, x_{t+1}) \\
 \text{BCE Loss} : \mathcal{L}_{\text{Decoder}} &= \mathcal{L}_1 + \mathcal{L}_2
 \end{aligned}
 \tag{3}$$

### A.4. Ranking based Evaluation Metrics - Hits at Rank 1 (H@1)

We follow the ranking-based metrics in latent spaces used in (Kipf et al., 2020; Goyal et al., 2020; 2021b; Ke et al., 2021), which is the Hit at rank 1 (H@1). This metric is introduced by (Kipf et al., 2020) with the definition of one hit when the predicted state representation is nearest to the encoded observation. We report the average number of hits over the test set. The higher H@1 score indicates a better model prediction.

## B. Reproducibility

Environment	Data points	Input frames	Num. Slots	Action Space	Epochs	Num. Mechanisms
2D Shapes	1k/10k/10k	1	5	4	100	5
3D Cubes	1k/10k/10k	1	5	4	100	5
Breakout	1k/100/100	3	3	4	200	5
Pong	1k/100/100	2	3	6	200	3
Balls	5k/1k/1k	2	3	0	100	7

Table 2: **Hyperparameters indication.** The number of Data points represents the size of the Train/Validation/Test sets,  $k$  abbreviated for 1000. The number of Mechanisms represents the chosen amount after validating.

### B.1. Datasets Generation

Follow (Kipf et al., 2020) a random policy is applied during generating datasets. The size of the training, validating, and test sets (the same for the iid and OOD test sets) are indicated in the second columns of Table 2.

As mentioned in Appendix A.1, we adjust the warmstart to generate the iid and OOD data sets for Atari games. For Pong, the warmstart is set to 58 and 100 for the iid and OOD data sets, respectively. The pair of warmstart for Breakout is 50 and 100.

## Reusable Slotwise Mechanisms

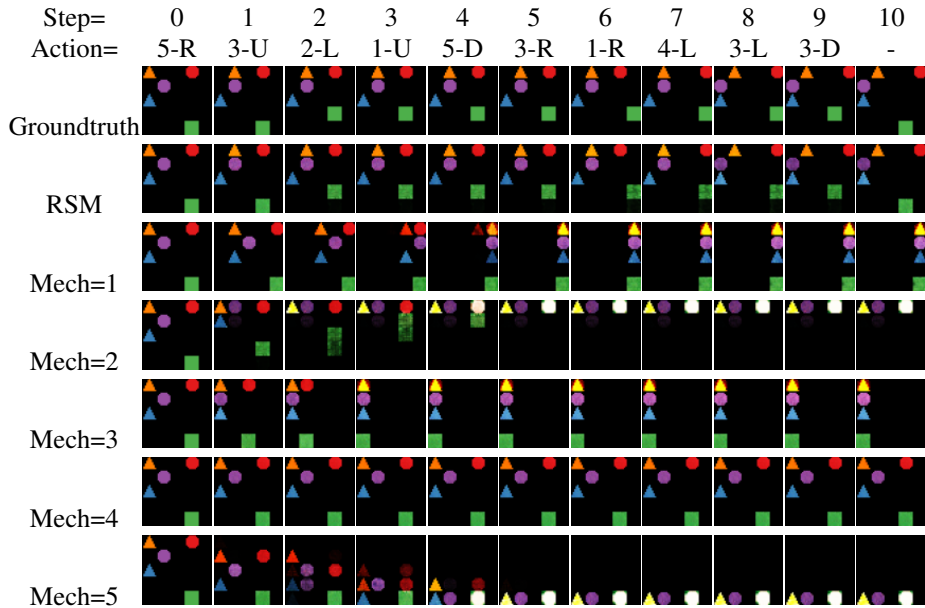


Figure 10: Observation of mechanisms assignment and mechanisms performance during 10 rolling out steps in 2D Shapes environment. The last 5 rows represent the reconstruction with a single mechanism assigned for all slots.

### B.2. Hyper-parameters

Most of the hyper-parameters used in this work are followed by C-SWM (Kipf et al., 2020). The rest of Table 2 summarizes the hyper-parameters for training and environment configurations. In addition, for all environments and methods, using the Adam optimizer (Kingma & Ba, 2015), a learning rate of  $5e - 4$ , batch size 1024, and hidden size 512. Follows (Kipf et al., 2020), each slot is encoded into a  $4 - dimension$  vector. After training the Encoder and the transition model, we train the Decoder for 100 epochs.

For the number of mechanisms in RSM, we trained models with 3, 5, and 7 mechanisms. Then, the chosen number is decided based on the result of the validation set over 30 random seeds. This number is the same for both the reported iid and OOD results and could be different among environments. In addition, in Appendix C.3, we further analyze the model performance in different numbers of mechanisms.

## C. Further discussion on the performance of each mechanism

### C.1. Observation on 2D Shapes

In Figure 10, we provide 10 steps which is the extended version of the analysis in Section 3.4. The analysis demonstrates the ability of RSM to generate correct reconstruction frames over 10 rolling-out prediction steps. The figure also exposure the stability of RSM in handling the required action in all cases of objects being allowed to move or being blocked by another object or one of the 4 walls.

Moreover, the analysis witnesses the strong points of mechanisms to learn distinct knowledge and consider well the particular situation to produce a proper actual response. For instance, the action moving to the LEFT is provided in steps 2 and 7 in cases where the purple round object is free to move at step 7 while the blue rectangle is blocked by the wall at step 2 and is not allowed to move. As we can see from the figure, mechanism 3 takes the manipulation LEFT but generates different actual movements on these 2 steps. In particular, mechanism 3 creates a *zero* modification to step 2 and moves the purple object to the left accurately.

However, it seems to be sensitive in cases of objects being blocked by another object in the last 5 rows when a single mechanism is applied to all slots at each prediction step. One reason comes from the difference in evaluation settings, there is only at most 1 slot is moved in the conventional flow during training and testing, while in this analysis, all slots are moved after each prediction step.

## C.2. Observation on Balls

In Figure 11, we illustrate the transformation of slots that are not governed by any action in Balls. First of all, RSM generates reasonable reconstructions over 10 steps prediction into the future, which are illustrated in row 3<sup>th</sup>. We observe that in different seeds and methods, slots in Balls capture the 3 balls and a circular trajectory. Next, looking at frame reconstructions with a single mechanism applied to all slots, we can see that all reconstructed frames are not suitable due to the missing objects or not correcting the object’s position compared to the ground-truth frame. Lastly, the following points describe some observations on the actual transformation produced by mechanisms from the reconstruction generated by a single mechanism:

**Observation 1:** mechanism performs a constant movement of slot-entity. Clearly illustrated in the figure, during 10 steps, slots do not change direction and seem to preserve the same velocities. However, directions and velocities are different among slots and mechanisms. Specifically, the circular trajectories move up or to some frame’s corner (upper); the groups of colored entities keep rotating by a pair of velocities in the 2D plane.

**Observation 2:** mechanism’s performance is different when applied to different slots. As we can see from the transformation of slots when mechanism 1 is applied, the circular trajectory in slot 1 keeps moving to the upper-right corner, whereas, slot 2 rotates counterclockwise and slot 3 slightly rotates or even does not move.

These observations not only encourage our hypothesis 2 that mechanisms learn different and meaningful knowledge but also demonstrate the reusability of mechanisms in RSM.

## C.3. Number of Mechanisms

In this section, we discuss the effect of the number of mechanisms on different environments. In Figure 12, we illustrate the changes in H@1 performance when the number of mechanisms is 3, 5, and 7 sequentially. We can observe an optimal number of mechanisms for each environment, which are [5, 5, 5, 3, 7] in the order from top to bottom. The performance drop in cases with less or more than the optimal number signals the requirement of redefining task complexity. For instance, from the Appendix C about Balls environment, we know that slots in Balls learn multiple circular trajectories. Therefore, a large number of mechanisms should be used to promote the model to handle more cases of trajectory and improve performance.

## D. Reconstruction Results

### D.1. Reconstruction in 3D Cubes environment

One of the challenges to generating reconstructions in 3D Cubes environment is to recognize the visibility order of objects. As visualized in Figure 15, RSM exposures the strength in communication among slots to obtain the order information, as well as generate the proper movement of slots and achieve an accurate reconstruction compared to the ground-truth. In contrast, MBRL misses that kind of information from the beginning steps and renders the blue, green, and yellow objects inside each other, then, witnesses a huge gap from the following steps to step 10. Besides, other methods lose the information of some objects and produce a not completed reconstruction at the end.

### D.2. Reconstruction in Pong environment

Figure 16 provides a problematic test case that contains a collision between the ball and the green paddle from step 1 to step 3, and the ball changes the movement direction in step 2. As illustrated in the figure, RSM produces the best reconstruction for the whole of 10 steps, which proves the benefit of information integration among slots in complex cases. More specifically, RSM recognizes and manages the collision well, and then, maintains the uniform motion of the ball after collision till the last step while handling the actions applied on the green paddle. MBRL also renders the three objects in Pong at the first 2 steps; however, it generates a ball that is blurred from step 3 and becomes hard to see at step 10. Other methods do not recognize the ball from the first step and show the loss of either the white or green paddle from step 7.

## E. Ablation Studies

We conduct ablation studies to emphasize the benefit of the communication flow proposed in RSM. As described in Section 3.5, the ablation studies in this work are listed as follows:

- RSM ab 01: the CCI is not used at step 2 but is used at step 3.
- RSM ab 10: the CCI is used at step 2 but is not used at step 3.
- RSM ab 00: the CCI is used at neither step 2 nor step 3.
- RSM ab par: the CCI is used at both step 2 and step 3, but wrapped in parallel updates instead of sequential order.

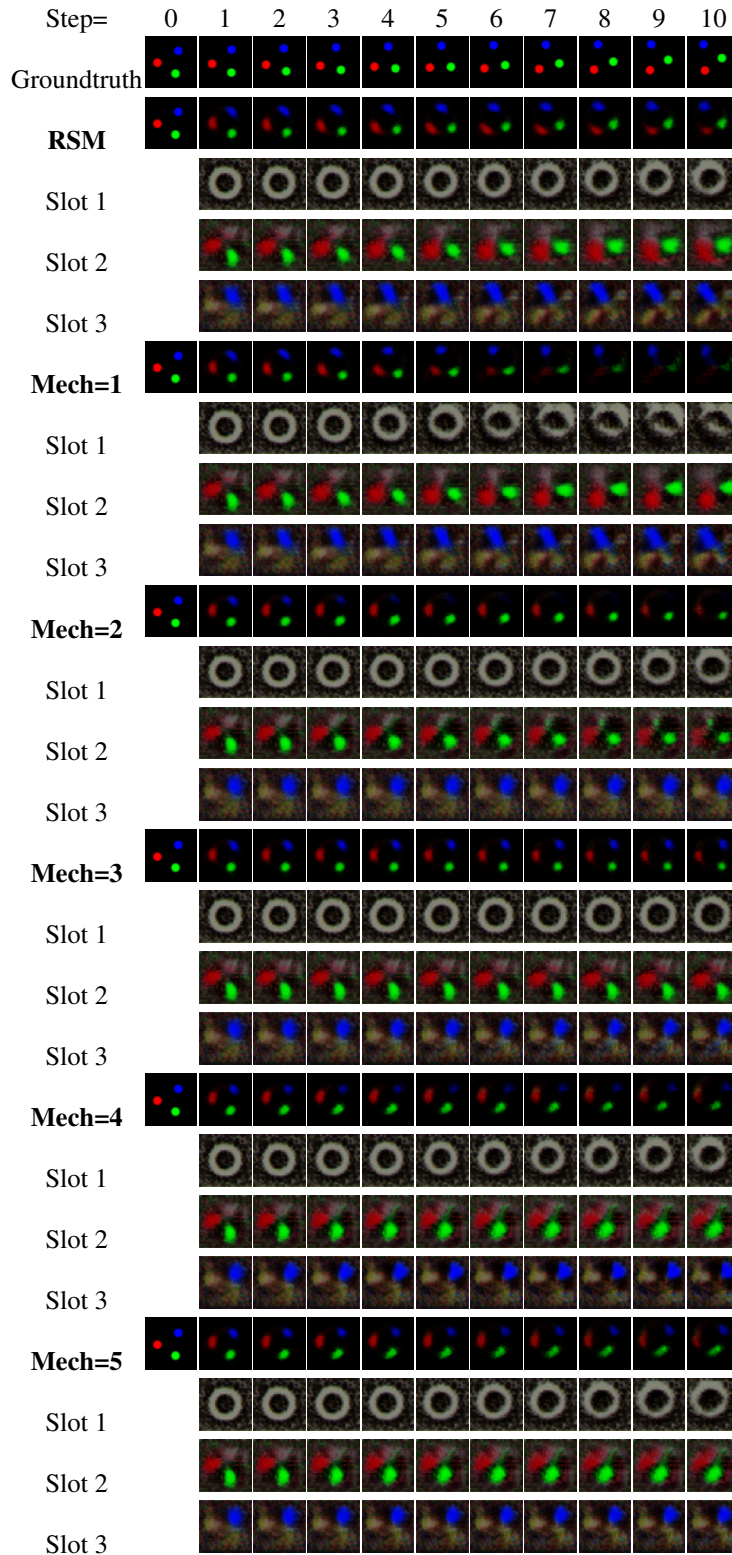
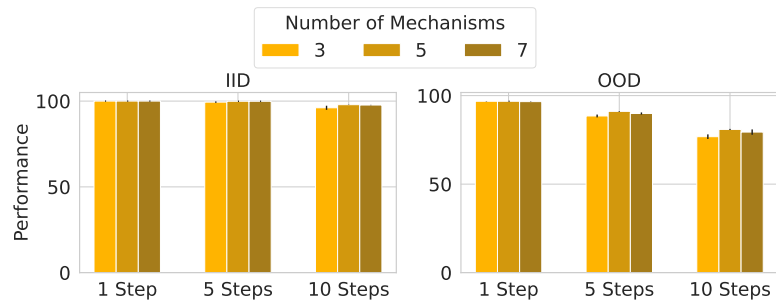


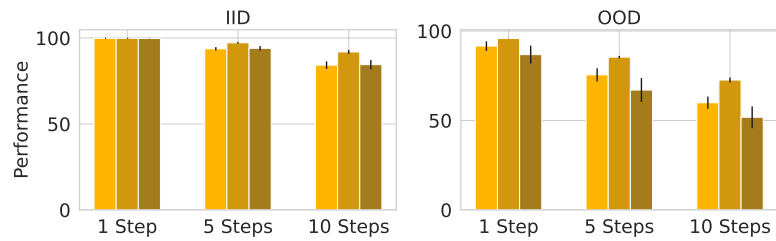
Figure 11: Observation of mechanisms assignment and mechanisms performance during 10 rolling out steps in Balls environment. The last 5 rows represent the reconstruction with a single mechanism assigned for all slots.



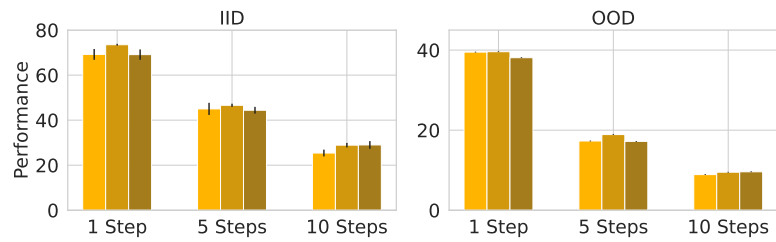
## Reusable Slotwise Mechanisms



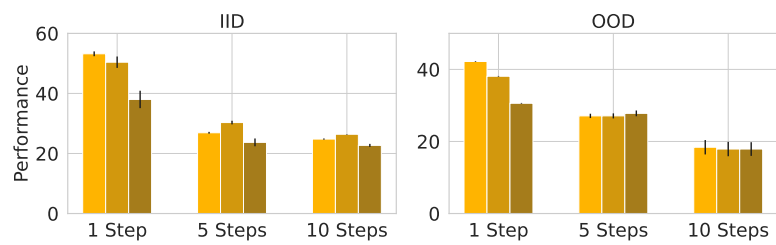
(a) 2D Shapes



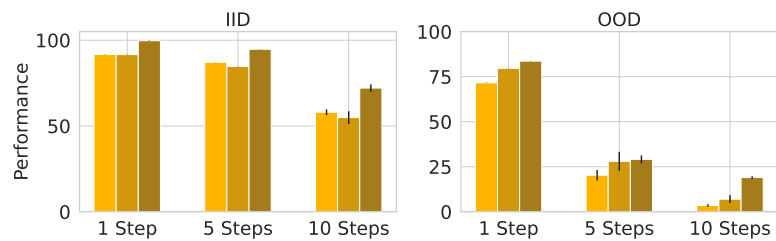
(b) 3D Cubes



(c) Breakout



(d) Pong



(e) Balls

Figure 12: Effects of number of mechanisms on H@1

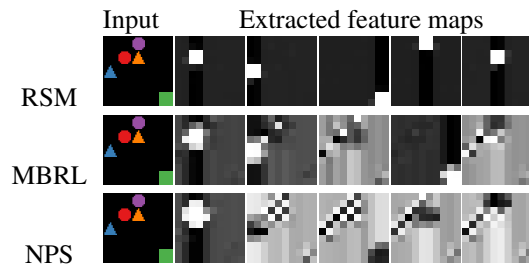


Figure 13: Comparison of extracted feature maps from a scene in 2D Shapes environment

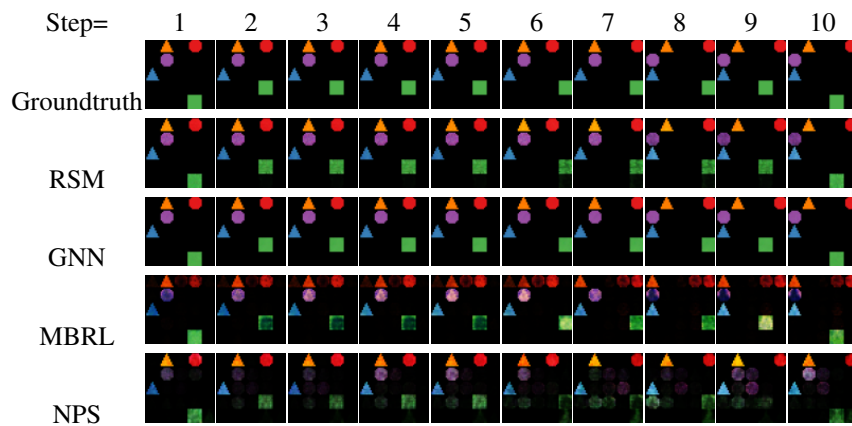


Figure 14: Reconstruction comparison on 2D Shapes dataset

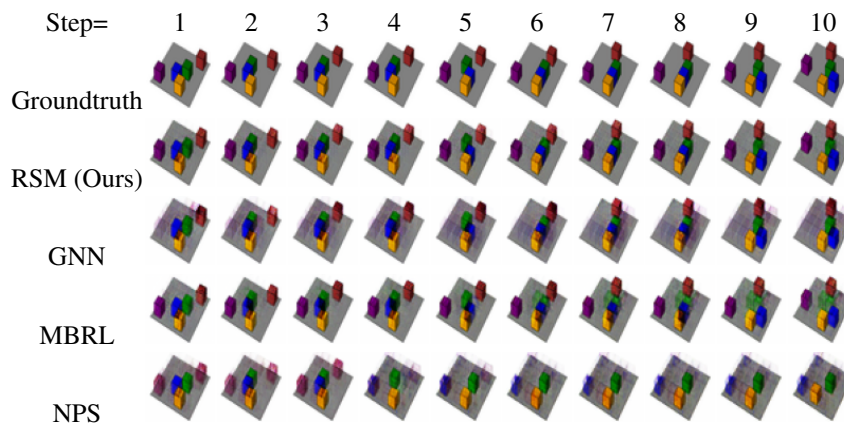


Figure 15: Reconstruction comparison on 3D Cubes dataset

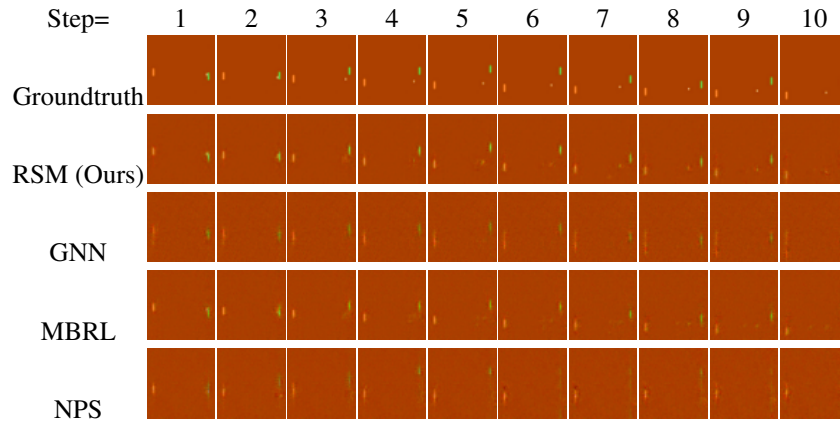


Figure 16: Reconstruction comparison on Pong dataset

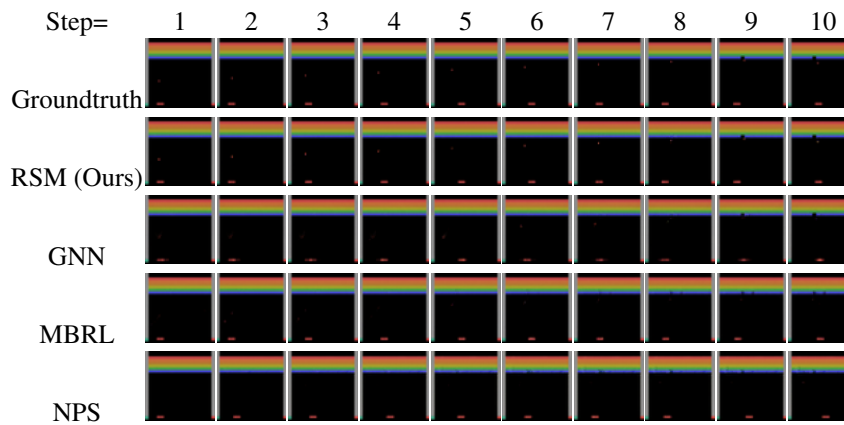


Figure 17: Reconstruction comparison on Breakout dataset

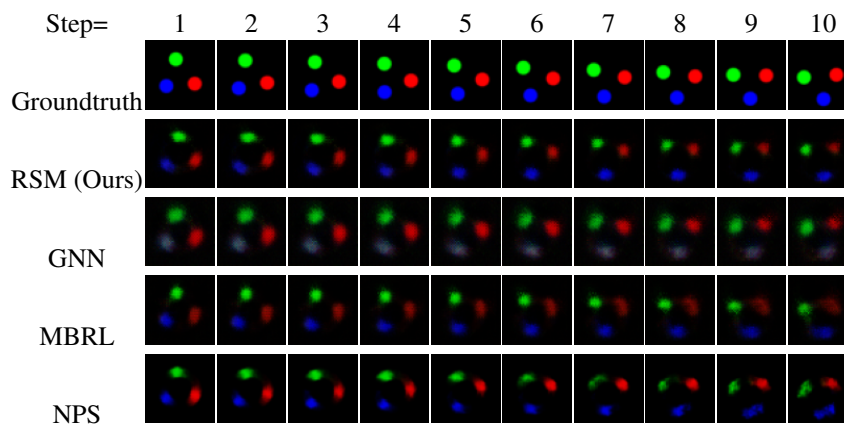


Figure 18: Reconstruction comparison on 3-Body Physic dataset

## Reusable Slotwise Mechanisms

---

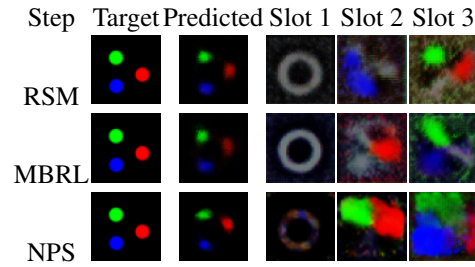


Figure 19: Comparison of the decoded slots at step 5 in the Balls environment

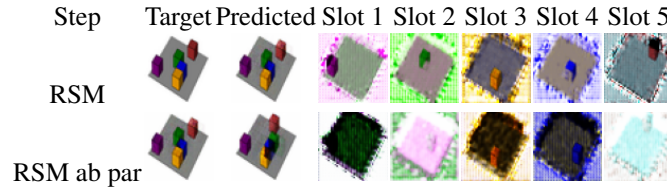


Figure 20: Comparison of the reconstructed slots at step 5 of the sequential and parallel version in the 3D Cubes environment. The parallel version misses the information visibility order due to the absence of information integration by the CCI in a sequential manner.

- MLP-CCI: the CCI is computed by an MLP instead of MultiheadAttention, then is used at both step 2 and step 3 in a sequential manner.

Table 3 represents the full comparison of the original design of RSM and the ablations. Overall, the results show that RSM exposure has the strongest result in both iid and OOD.

In addition, Figure 20 provides the comparison of RSM and the absence of sequential information integration.



Table 3: **Comparison on ablation studies.** The reported scores are mean and standard error over 30 seeds of ranking scores for multi-step prediction into the future. The higher scores indicate a better prediction. The best scores are **bolded**.

		IID			OOD		
		<i>1 step</i>	<i>5 steps</i>	<i>10 steps</i>	<i>1 step</i>	<i>5 steps</i>	<i>10 steps</i>
Shapes	RSM (Ours)	<b>100.0</b> ±0.0	<b>99.9</b> ±0.0	<b>97.9</b> ±0.1	<b>96.8</b> ±0.0	<b>91.1</b> ±0.2	<b>80.9</b> ±0.3
	RSM ab 01	<b>100.0</b> ±0.0	99.0±0.4	94.7±1.3	96.7±0.1	86.4±1.4	71.8±2.9
	RSM ab 10	<b>100.0</b> ±0.0	<b>99.9</b> ±0.0	97.4±0.1	96.9±0.0	89.9±0.3	79.6±0.6
	RSM ab 00	<b>100.0</b> ±0.0	98.8±0.0	90.5±0.1	96.8±0.0	77.7±0.4	52.4±0.8
	RSM ab par	<b>100.0</b> ±0.0	<b>99.9</b> ±0.0	97.5±0.1	96.7±0.1	90.2±0.4	80.2±0.5
	MLP-CCI	<b>100.0</b> ±0.0	94.8±0.0	89.8±0.1	95.6±0.2	86.1±0.4	70.3±1.0
Cubes	RSM (Ours)	99.8±0.0	<b>99.2</b> ±0.6	<b>93.9</b> ±1.5	<b>97.5</b> ±0.2	<b>89.6</b> ±0.9	<b>77.5</b> ±1.5
	RSM ab 01	99.8±0.0	94.7±0.8	86.0±2.1	94.6±0.3	80.9±1.4	65.2±1.8
	RSM ab 10	<b>100.0</b> ±0.0	98.0±0.7	93.8±1.7	96.0±0.1	84.4±0.6	69.0±0.9
	RSM ab 00	<b>100.0</b> ±0.0	91.9±0.7	82.5±1.6	94.4±0.5	72.6±1.3	48.0±2.8
	RSM ab par	99.8±0.0	95.5±0.6	87.4±1.3	94.8±0.5	80.6±1.5	65.7±1.9
	MLP-CCI	99.7±0.0	87.8±0.3	81.7±0.6	93.6±0.3	80.6±1.0	60.4±1.5
Breakout	RSM (Ours)	73.3±1.0	46.6±1.7	27.2±2.0	<b>39.8</b> ±0.1	<b>19.1</b> ±0.4	<b>10.1</b> ±1.2
	RSM ab 01	69.3±2.6	39.8±3.0	23.4±3.1	22.3±2.1	4.0±0.7	2.1±0.7
	RSM ab 10	<b>74.5</b> ±1.4	<b>54.5</b> ±2.8	<b>32.9</b> ±2.3	22.8±2.2	4.4±0.9	2.2±0.5
	RSM ab 00	46.3±4.1	25.3±2.8	18.8±2.1	20.0±1.8	5.1±0.6	2.6±0.5
	RSM ab par	72.5±0.9	41.6±1.7	22.4±1.0	22.1±1.4	5.5±0.6	2.5±0.6
	MLP-CCI	70.1±1.5	39.3±3.0	23.9±2.6	29.2±4.0	6.3±0.5	3.2±0.7
Pong	RSM (Ours)	<b>53.9</b> ±1.5	<b>30.6</b> ±1.0	<b>23.5</b> ±0.7	<b>41.6</b> ±0.8	<b>24.8</b> ±1.6	<b>18.6</b> ±2.1
	RSM ab 01	43.5±3.1	21.3±1.1	15.0±1.4	15.2±2.5	2.5±0.3	2.2±0.3
	RSM ab 10	44.9±4.3	24.3±2.2	20.7±2.5	26.7±3.5	13.1±0.2	11.8±0.4
	RSM ab 00	41.8±5.7	20.5±4.9	18.7±4.1	9.7±4.3	2.7±0.5	1.3±0.3
	RSM ab par	50.4±3.4	24.3±1.6	20.9±1.2	18.1±2.7	2.1±0.4	1.9±0.5
	MLP-CCI	45.9±3.3	24.1±2.5	18.1±2.3	15.2±2.8	3.1±0.5	1.9±0.5
Balls	RSM (Ours)	<b>99.8</b> ±0.0	<b>92.9</b> ±1.8	72.6±4.5	<b>84.3</b> ±1.9	<b>28.3</b> ±4.2	<b>19.6</b> ±2.4
	RSM ab 01	99.6±0.1	89.2±3.7	68.8±5.9	81.2±1.4	12.1±0.9	4.1±0.5
	RSM ab 10	99.7±0.0	93.2±1.1	68.8±2.4	83.2±1.4	12.7±1.8	5.1±0.8
	RSM ab 00	<b>99.8</b> ±0.0	92.8±0.9	67.9±2.3	82.9±1.5	13.1±1.8	4.4±0.8
	RSM ab par	99.7±0.0	90.7±2.7	69.8±5.6	80.3±2.2	11.9±3.4	4.5±1.6
	MLP-CCI	99.8±0.0	90.3±1.2	71.2±3.3	84.6±3.4	21.3±4.7	7.0±2.5